Available online at www.sciencedirect.com

ScienceDirect

International Journal of Solids and Structures 43 (2006) 6488–6501

INTERNATIONAL JOURNAL OF SOLIDS and STRUCTURES

www.elsevier.com/locate/ijsolstr

Dynamic limit analysis formulation for impact simulation of structural members

Kee Poong Kim [a], Hoon Huh [b,*]

[a] *Micro Mold & Die Team, Korea Institute of Industrial Technology, 971-35, Wolchul-dong, Buk-gu, Gwangju, 500-460, Republic of Korea*
[b] *Department of Mechanical Engineering, Korea Advanced Institute of Science and Technology, 373-1, Guseong-dong, Yuseong-gu, Daejeon 305-701, Republic of Korea*

Received 14 June 2005; received in revised form 8 December 2005
Available online 26 January 2006

Abstract

This paper introduces an extended concept of limit analysis to deal with the dynamic equilibrium condition considering the inertia and strain-rate effect for dynamic behavior of structures. The conventional limit analysis method has been applied to only static collapse analysis of structures without consideration of dynamic effects in the structural behavior. A dynamic formulation for the limit analysis has been derived for incremental analysis dealing with time integration, strain and stress evaluation, strain hardening, strain-rate hardening and thermal softening. The time dependent term in the governing equation is integrated with the WBZ-α method. The dynamic material behavior is described by the Johnson–Cook model in order to consider strain-rate hardening and thermal softening as well as strain hardening. Simulations have been carried out for impact analysis of a Taylor bar and an S-rail and their numerical results are compared with elasto-plastic explicit analysis results by LS-DYNA3D. Comparison demonstrates that the dynamic finite element limit analysis can predict the crashworthiness of structural members effectively with less effort and computing time than the commercial code compared. The crashworthiness of a structure with the rate-dependent constitutive model is also compared to that with the quasi-static constitutive relation in order to investigate the dynamic effect on deformation of structures.

Keywords: Finite element limit analysis; Dynamic limit analysis formulation; Structural impact; Strain-rate hardening

1. Introduction

Structural members of a vehicle are designed to increase the energy absorption efficiency and thus to enhance the safety and reliability of a vehicle. The crashworthiness of each member needs to be evaluated at the initial stage of vehicle design for good performance of an assembled vehicle. As the dynamic behavior of structural members is different from the static one, the crashworthiness of vehicle structures has to be assessed by impact analysis considering the dynamic response related to the inertia and strain-rate hardening

* Corresponding author. Tel.: +82 42 869 3222; fax: +82 42 869 3210.
E-mail address: hhuh@kaist.ac.kr (H. Huh).

0020-7683/$ - see front matter
doi:10.1016/j.ijsolstr.2005.12.004

effect. Impact simulation is usually carried out with the elastic-plastic finite element analysis code such as PAMCRASH or LS-DYNA3D. It inevitably requires tremendous time and efforts to estimate the crashworthiness of structural members even with the explicit methods. An efficient, alternative analysis tool could be an extended limit method for fast evaluation of the crashworthiness of structural members.

Limit analysis has become a useful and efficient numerical tool in the collapse behavior assessment for structural members since the method can easily calculate the plastic collapse load, the energy absorption rate and the deformation mode at incipient collapse with the rigorous mathematical formulation and efficient computational methodology (Anderheggen and Knöpfel, 1972; Dang Hung, 1976; Christiansen, 1981; Huh and Yang, 1991). The limit analysis method has been greatly fortified with various capable aspects of automatic mesh refinement, general yield conditions, anisotropic materials and shell elements (Christiansen and Pedersen, 2001; Christiansen and Andersen, 1999; Ponter et al., 2000; Capsoni et al., 2001; Huh et al., 2001). A burst of development in limit theories and computer technologies enable limit analysis applied to complicated structural problems (Kim and Huh, 1999). The limit analysis concept has extended to a class of work-hardening materials from its long conjecture of perfectly plastic materials (Huh et al., 1999). Although the algorithm with a simple formulation has the advantage of stable convergence, computational efficiency and easy access to work-hardening materials, the method has been developed only for static collapse behavior of structures. Development of dynamic limit analysis could make it possible to evaluate the crashworthiness of structural members efficiently and systematically.

In this paper, the limit analysis concept is extended to incorporate with the dynamic equilibrium condition considering the inertia and strain-rate effects instead of the static equilibrium. A dynamic formulation of limit analysis has been derived for sequential incremental analysis dealing with time integration, strain and stress evaluation, strain hardening, strain-rate hardening and thermal softening. The time dependent term in the governing equation is integrated with the WBZ-α method proposed by Wood et al. (1981). The dynamic material behavior is described by the Johnson–Cook model (Johnson and Cook, 1983) in order to consider strain-rate hardening and thermal softening as well as strain hardening. The analysis method developed has been applied to a class of impact analysis of structural members. Two typical problems have been considered: one is the impact deformation of a Taylor bar as bulk deformation with the use of solid elements; and the other is the crush deformation of an S-rail as thin-wall deformation with the use of shell elements. Numerical results are compared with elasto-plastic explicit analysis results by LS-DYNA3D for collapse loads and its deformed shapes as well as the strain distribution. Comparison demonstrates that the dynamic finite element limit analysis can predict the crashworthiness of structural members effectively with less effort and computing time than the commercial codes compared. The crashworthiness of the structure with the rate-dependent constitutive model is also compared to that with the quasi-static constitutive relation in order to investigate the dynamic effect on deformation of structures.

2. Dynamic formulation of limit analysis

2.1. Dynamic limit analysis theory

The limit analysis formulation consists of a primal and dual formulation. The primal formulation for the limit analysis considering dynamic effects can be derived from the dynamic equilibrium equations, the static boundary condition and the yield condition in the form of a constrained maximization problem:

$$\begin{aligned} &\text{maximize} && q(\sigma) \\ &\text{subject to} && \nabla \cdot \sigma = \rho \boldsymbol{a} \quad \text{in } D \\ &&& \sigma \cdot \boldsymbol{n} = q\boldsymbol{t} \quad \text{on } \partial D_S \\ &&& \|\sigma\|_{(v)} \leqslant \sigma_0 \quad \text{in } D \end{aligned} \tag{1}$$

where σ is the stress tensor in the reference domain D, $\boldsymbol{t}$ is the traction force vector on the boundary surface ∂D_S whose unit outer normal vector is $\boldsymbol{n}$, q is a positive real parameter of proportional loading, ρ is the density of material and $\boldsymbol{a}$ is the acceleration vector. The norm expression with inequality identifies a plastic material that obeys the convex yield criterion and the associated flow rule. Introduction of the acceleration term $\boldsymbol{a}$ may

not seem to be proper in terms of a primal formulation which deals only with the statically admissible set and constitutively admissible set. In this case, the term could be regarded as an inertial force or reversed effective force as the D'Alembert's Principle says. The term is, however, necessary for a dual formulation as a time-dependent and rate-dependent problem. The convex primal formulation has its dual one that corresponds to an upper bound formulation. To construct the dual formulation, the principle of virtual work is used to form a weak formulation from the equilibrium equations.

$$\int_D \boldsymbol{v} \cdot (\nabla \cdot \sigma)\,\mathrm{d}\Omega = \int_D \rho \boldsymbol{a} \cdot \boldsymbol{v}\,\mathrm{d}\Omega, \quad \forall \boldsymbol{v} \tag{2}$$

where $\boldsymbol{v}$ is an arbitrary function with the physical interpretation as an admissible velocity function. The admissible $\boldsymbol{v}$, which satisfies the kinematic boundary conditions on ∂D_K, will lead to the equivalent variational statement by applying the divergence theorem and static boundary conditions,

$$\int_D \sigma : \dot{\varepsilon}\,\mathrm{d}\Omega + \int_D \rho \boldsymbol{a} \cdot \boldsymbol{v}\,\mathrm{d}\Omega = q \int_{\partial D_S} \boldsymbol{t} \cdot \boldsymbol{v}\,\mathrm{d}\Gamma \tag{3}$$

where $\dot{\varepsilon}$ is the strain rate and the symbol ':' denotes the inner product operator between two tensors. Eq. (3) can be restated in an alternative statement

$$q(\sigma) = \int_D \sigma : \dot{\varepsilon}\,\mathrm{d}\Omega + \int_D \rho \boldsymbol{a} \cdot \boldsymbol{v}\,\mathrm{d}\Omega \tag{4}$$

after the normalization of the boundary integral in Eq. (3) such that

$$\int_{\partial D_S} \boldsymbol{t} \cdot \boldsymbol{v}\,\mathrm{d}\Gamma = 1 \tag{5}$$

The term $\sigma : \dot{\varepsilon}$ can be restated by the principle of the maximum plastic work dissipation or by a generalized Hölder inequality.

$$\sigma : \dot{\varepsilon} = |\sigma : \dot{\varepsilon}| \leqslant \|\sigma\|_{(v)} \|\dot{\varepsilon}\|_{(-v)} = \bar{\sigma}\bar{\dot{\varepsilon}} \tag{6}$$

where $\|\sigma\|_{(v)}$ denotes the von-Mises norm of the stress and $\|\dot{\varepsilon}\|_{(-v)}$ denotes the minus von-Mises norm of the strain rate, which define the equivalent stress and strain rate, respectively. Consequently, an upper bound to the functional, $q(\sigma)$, can be established through the sequence of inequalities as

$$\begin{aligned} q(\sigma) &= \int_D \sigma : \dot{\varepsilon}\,\mathrm{d}\Omega + \int_D \rho \boldsymbol{a} \cdot \boldsymbol{v}\,\mathrm{d}\Omega \\ &= \int_D |\sigma : \dot{\varepsilon}|\,\mathrm{d}\Omega + \int_D \rho \boldsymbol{a} \cdot \boldsymbol{v}\,\mathrm{d}\Omega \\ &\leqslant \int_D \|\sigma\|_{(v)} \|\dot{\varepsilon}\|_{(-v)}\,\mathrm{d}\Omega + \int_D \rho \boldsymbol{a} \cdot \boldsymbol{v}\,\mathrm{d}\Omega \\ &\leqslant \sigma_0 \int_D \|\dot{\varepsilon}\|_{(-v)}\,\mathrm{d}\Omega + \int_D \rho \boldsymbol{a} \cdot \boldsymbol{v}\,\mathrm{d}\Omega \\ &= \tilde{q}(\boldsymbol{v}) \end{aligned} \tag{7}$$

where the upper bound functional $\tilde{q}(\boldsymbol{v})$ depends only on the kinematically admissible function $\boldsymbol{v}$. Based on the inequality in Eq. (7) and the existence of the absolute minimum of $\tilde{q}(\boldsymbol{v})$, the dual formulation may be stated as

$$\begin{aligned} &\text{minimize} \quad \tilde{q}(\boldsymbol{v}) \\ &\text{subject to} \quad \tilde{q} = \sigma_0 \int_D \|\dot{\varepsilon}\|_{(-v)}\,\mathrm{d}\Omega + \int_D \rho \boldsymbol{a} \cdot \boldsymbol{v}\,\mathrm{d}\Omega \\ &\qquad\qquad \int_{\partial D_S} \boldsymbol{t} \cdot \boldsymbol{v}\,\mathrm{d}\Gamma = 1 \\ &\qquad\qquad \mathrm{Tr}(\dot{\varepsilon}) = 0 \\ &\qquad\qquad \text{Kinematic boundary conditions} \end{aligned} \tag{8}$$

where the third equation in the constraint is obtained from the incompressibility condition. The dual formulation (8) is very similar to sequential limit analysis which was introduced by Huh and Yang (1991) except it is modified with the addition of the inertial term. In real problems, a general solution of formulation (8) could be obtained in the form of the dynamic collapse load, the corresponding dynamic collapse mode and the accumulated deformed shape with a proper numerical algorithm of time integration and sequential limit analysis which will be discussed in the next two sections.

In order to simulate the dynamic behavior of a general hardening material, the initial yield stress, σ_0, is replaced by the current yield stress, $\bar{\sigma}$, and the current yield stress from the flow stress curve is considered as a step-wise constant for each dual solution. The current yield stress, $\bar{\sigma}$, which is updated based on the effective plastic strain, the effective plastic strain rate and temperature, calculated from successive iterations using the bisection method (Huh et al., 1999). The yield stress in the ith iteration can be calculated from the iteration formula,

$$\bar{\sigma}^{(i)} = \frac{\bar{\sigma}^{(i-1)} + \bar{\sigma}_0}{2} \tag{9}$$

where $\bar{\sigma}_0$ is the yield stress determined in the previous time step and $\bar{\sigma}^{(i-1)}$ is the calculated yield stress at each iterative step with a hardening function of $\bar{\sigma} = H(\bar{\varepsilon}, \dot{\bar{\varepsilon}}, T)$. $H(\bar{\varepsilon}, \dot{\bar{\varepsilon}}, T)$ represents a function of the strain hardening, the strain rate hardening and the thermal softening. One typical hardening function is the Johnson–Cook model which is expressed as

$$\bar{\sigma} = (A + B\bar{\varepsilon}^n)\left[1 + C\ln\left(\frac{\dot{\bar{\varepsilon}}}{\dot{\bar{\varepsilon}}_0}\right)\right](1 - T^{*m}) \tag{10}$$

where A, B, n, C and m are material constants, $\dot{\bar{\varepsilon}}$ is the equivalent strain rate, $\dot{\bar{\varepsilon}}_0$ is the reference value of the equivalent strain rate, and T^* is the homologous temperature given by

$$T^* = \frac{T - T_{\text{room}}}{T_{\text{melt}} - T_{\text{room}}} \tag{11}$$

2.2. Finite dimensional approximation and minimization procedure

The dual formulation is discretized into the sub-domain of the finite element and reduced to a finite dimensional convex problem. The objective functional in Eq. (8) can be expressed with the incompressibility condition imposed as follows:

$$\tilde{q} = \sum_{e=1}^{E} \bar{\sigma} \int_{D_e} \|\dot{\varepsilon}\|_{(-v)}\, \mathrm{d}\Omega + \Lambda \sum_{e=1}^{E} \int_{D_e} (\dot{\varepsilon}_{ii})^2\, \mathrm{d}\Omega + \sum_{e=1}^{E} \int_{D_e} \rho \boldsymbol{a} \cdot \boldsymbol{v}\, \mathrm{d}\Omega \tag{12}$$

where Λ is a penalty number for the incompressibility condition considered for solid elements. The second term in Eq. (12) is not considered for shell elements since the incompressibility condition is included in the effective strain rate due to assumption that the stress component normal to the mid-surface is zero based on the shell theory. Instead, the incompressibility condition is imposed when the thickness strain is calculated from the in-plane strains.

The effective strain rate in Eq. (12) can be expressed by the von-Mises yield criterion generally as

$$\|\dot{\varepsilon}\|_{(-v)} = \dot{\bar{\varepsilon}} = \sqrt{\frac{2}{3}\dot{\varepsilon}_{ij}\dot{\varepsilon}_{ij}} \tag{13}$$

The effective strain rate in Eq. (13) can be rewritten in a matrix form as

$$\|\dot{\varepsilon}\|_{(-v)} = \left[\frac{2}{3}\dot{\boldsymbol{E}}^{\mathrm{T}}\boldsymbol{G}_1\dot{\boldsymbol{E}}\right]^{1/2} = \left[\frac{2}{3}\dot{\boldsymbol{U}}^{\mathrm{T}}\boldsymbol{B}^{\mathrm{T}}\boldsymbol{G}_1\boldsymbol{B}\dot{\boldsymbol{U}}\right]^{1/2} = [\dot{\boldsymbol{U}}^{\mathrm{T}}\overline{\boldsymbol{K}}_{e1}\dot{\boldsymbol{U}}]^{1/2} \tag{14}$$

where $\dot{\boldsymbol{E}}$ is the strain rate vector for each finite element, $\dot{\boldsymbol{U}}$ is the nodal velocity vector. $\boldsymbol{B}$ is a matrix for a relation between the velocity vector and effective strain rate, which is derived from the general finite element

theory. $\boldsymbol{G}_1$ is a constant matrix denoting a relation between strain rate components and the effective strain rate in the von-Mises yield condition as follows (Kim and Huh, 1999; Huh et al., 2001):

$$\boldsymbol{G}_1 = \begin{bmatrix} 1 & 0 & 0 & 0 & 0 & 0 \\ 0 & 1 & 0 & 0 & 0 & 0 \\ 0 & 0 & 1 & 0 & 0 & 0 \\ 0 & 0 & 0 & 2 & 0 & 0 \\ 0 & 0 & 0 & 0 & 2 & 0 \\ 0 & 0 & 0 & 0 & 0 & 2 \end{bmatrix} \quad \text{for solid elements} \tag{15}$$

$$\boldsymbol{G}_1 = \begin{bmatrix} 2 & 1 & 0 & 0 & 0 \\ 1 & 2 & 0 & 0 & 0 \\ 0 & 0 & 2 & 0 & 0 \\ 0 & 0 & 0 & 2 & 0 \\ 0 & 0 & 0 & 0 & 2 \end{bmatrix} \quad \text{for shell elements} \tag{16}$$

The matrix form for the incompressibility condition in Eq. (12) for solid elements can be written as

$$(\dot{\varepsilon}_{ii})^2 = (\dot{\varepsilon}_x + \dot{\varepsilon}_y + \dot{\varepsilon}_z)^2 = \dot{\boldsymbol{U}}^{\mathrm{T}}\boldsymbol{B}^{\mathrm{T}}\boldsymbol{G}_2\boldsymbol{B}\dot{\boldsymbol{U}} = \dot{\boldsymbol{U}}^{\mathrm{T}}\overline{\boldsymbol{K}}_{e2}\dot{\boldsymbol{U}} \tag{17}$$

where

$$\boldsymbol{G}_2 = \begin{bmatrix} 1 & 1 & 1 & 0 & 0 & 0 \\ 1 & 1 & 1 & 0 & 0 & 0 \\ 1 & 1 & 1 & 0 & 0 & 0 \\ 0 & 0 & 0 & 0 & 0 & 0 \\ 0 & 0 & 0 & 0 & 0 & 0 \\ 0 & 0 & 0 & 0 & 0 & 0 \end{bmatrix} \quad \text{for solid elements} \tag{18}$$

The inertia term can be expressed in the matrix form as follows:

$$\sum_{e=1}^{E} \int_{D_e} \rho \boldsymbol{a} \cdot \boldsymbol{v} \, \mathrm{d}\Omega = \sum_{e=1}^{E} \ddot{\boldsymbol{U}}^{\mathrm{T}}\boldsymbol{M}_e\dot{\boldsymbol{U}} = \ddot{\boldsymbol{U}}^{\mathrm{T}}\boldsymbol{M}\dot{\boldsymbol{U}} \tag{19}$$

where $\ddot{\boldsymbol{U}}$ is the nodal acceleration vector and $\boldsymbol{M}$ is the mass matrix.

The normalization condition in Eq. (8) can be discretized as follows:

$$\boldsymbol{C}^{\mathrm{T}}\dot{\boldsymbol{U}} = 1 \tag{20}$$

An approximation of the dual formulation with Eqs. (14), (17), (19) and (20) becomes a constrained minimization problem,

$$\begin{aligned} &\text{minimize} \quad \tilde{q}(\dot{\boldsymbol{U}}) = \sum_{e=1}^{E} \bar{\sigma} \int_{D_e} \sqrt{\dot{\boldsymbol{U}}^{\mathrm{T}}\overline{\boldsymbol{K}}_{e1}\dot{\boldsymbol{U}}} \, \mathrm{d}\Omega + \Lambda \sum_{e=1}^{E} \int_{D_e} \dot{\boldsymbol{U}}^{\mathrm{T}}\overline{\boldsymbol{K}}_{e2}\dot{\boldsymbol{U}} \, \mathrm{d}\Omega + \ddot{\boldsymbol{U}}^{\mathrm{T}}\boldsymbol{M}\dot{\boldsymbol{U}} \\ &\text{subject to} \quad \boldsymbol{C}^{\mathrm{T}}\dot{\boldsymbol{U}} = 1 \end{aligned} \tag{21}$$

The above constrained minimization problem is converted into an unconstrained one with the Lagrange multiplier method such that

$$\text{minimize} \quad \Phi(\dot{\boldsymbol{U}}, \lambda) = \sum_{e=1}^{E} \bar{\sigma} \int_{D_e} \sqrt{\dot{\boldsymbol{U}}^{\mathrm{T}}\overline{\boldsymbol{K}}_{e1}\dot{\boldsymbol{U}}} \, \mathrm{d}\Omega + \Lambda \sum_{e=1}^{E} \int_{D_e} \dot{\boldsymbol{U}}^{\mathrm{T}}\overline{\boldsymbol{K}}_{e2}\dot{\boldsymbol{U}} \, \mathrm{d}\Omega + \ddot{\boldsymbol{U}}^{\mathrm{T}}\boldsymbol{M}\dot{\boldsymbol{U}} - \lambda(\boldsymbol{C}^{\mathrm{T}}\dot{\boldsymbol{U}} - 1) \tag{22}$$

Differentiating Eq. (22) with respect to the velocity vector and the Lagrange multiplier results in the following equations:

$$\begin{aligned}&\frac{\partial \Phi}{\partial \dot{\boldsymbol{U}}}=0; \quad \sum_{e=1}^{E}\bar{\sigma}\int_{D_e}\frac{\overline{\boldsymbol{K}}_{e1}\dot{\boldsymbol{U}}}{\sqrt{\dot{\boldsymbol{U}}^{\mathrm{T}}\overline{\boldsymbol{K}}_{e1}\dot{\boldsymbol{U}}}}\,\mathrm{d}\Omega+\Lambda\sum_{e=1}^{E}\int_{D_e}\overline{\boldsymbol{K}}_{e2}\dot{\boldsymbol{U}}\,\mathrm{d}\Omega+\boldsymbol{M}\ddot{\boldsymbol{U}}=\lambda\boldsymbol{C}\\&\frac{\partial \Phi}{\partial \lambda}=0; \quad \boldsymbol{C}^{\mathrm{T}}\dot{\boldsymbol{U}}=1\end{aligned} \tag{23}$$

The stiffness matrix in Eq. (23) can be modified as an iteration form by replacing the velocity field in the denominator with the one obtained in the previous iterative step, that is,

$$\boldsymbol{K}_i=\sum_{e=1}^{E}\bar{\sigma}\int_{D_e}\frac{\overline{\boldsymbol{K}}_{e1}}{\sqrt{\dot{\boldsymbol{U}}_{i-1}^{\mathrm{T}}\overline{\boldsymbol{K}}_{e1}\dot{\boldsymbol{U}}_{i-1}}}\,\mathrm{d}\Omega+\Lambda\sum_{e=1}^{E}\int_{D_e}\overline{\boldsymbol{K}}_{e2}\,\mathrm{d}\Omega \tag{24}$$

It leads to a problem of solving matrix equations in each iterative step such that

$$\begin{aligned}&\boldsymbol{K}\dot{\boldsymbol{U}}+\boldsymbol{M}\ddot{\boldsymbol{U}}=\lambda\boldsymbol{C}\\&\boldsymbol{C}^{\mathrm{T}}\dot{\boldsymbol{U}}=1\end{aligned} \tag{25}$$

The solution of Eq. (25) can be obtained incorporating with the time integration scheme for the velocity and acceleration term. The kinematic boundary conditions are imposed in the time integration step.

2.3. Solution method with time integration

The time dependent terms in Eq. (25) are integrated with the WBZ-α method which proposed by Wood et al. (1981). The WBZ-α method to solve Eq. (25) has the form as follows

$$\begin{aligned}&\boldsymbol{K}\dot{\boldsymbol{U}}_n+(1-\alpha)\boldsymbol{M}\ddot{\boldsymbol{U}}_n+\alpha\boldsymbol{M}\ddot{\boldsymbol{U}}_{n-1}=\lambda_n\boldsymbol{C}\\&\boldsymbol{C}^{\mathrm{T}}\dot{\boldsymbol{U}}_n=1\\&\boldsymbol{U}_n=\boldsymbol{U}_{n-1}+\Delta t\dot{\boldsymbol{U}}_{n-1}+\frac{1}{2}\Delta t^2[(1-2\beta)\ddot{\boldsymbol{U}}_{n-1}+2\beta\ddot{\boldsymbol{U}}_n]\\&\dot{\boldsymbol{U}}_n=\dot{\boldsymbol{U}}_{n-1}+\Delta t[(1-\gamma)\ddot{\boldsymbol{U}}_{n-1}+\gamma\ddot{\boldsymbol{U}}_n]\end{aligned} \tag{26}$$

where $n-1$ and n indicate the previous and current time step respectively, and Δt denotes the time step size. The method is implicit and known to be unconditionally stable with the second order accuracy for the following conditions

$$\beta=\frac{1}{4}(1-\alpha)^2, \quad \gamma=\frac{1}{2}-\alpha \tag{27}$$

In Eqs. (26) and (27), α is a parameter to control high-frequency oscillation, which is selected in the range of

$$-1\leqslant\alpha\leqslant 0 \tag{28}$$

When $\alpha=0$, the method reduces to the trapezoidal rule which has no numerical dissipation. As the value of α decreases, the amount of numerical damping increases. When $\alpha=-1$, the WBZ-α method is asymptotically annihilating. In this paper, the dissipation parameter, α, is set to the value of −0.3 through numerical tests in order to consider the effective high-frequency dissipation without loss of the accuracy of a solution.

The time integration scheme in Eq. (26) rewrites the Eq. (25) as

$$\begin{aligned}&\tilde{\boldsymbol{K}}\dot{\boldsymbol{U}}_n=\lambda_n\boldsymbol{C}+\boldsymbol{R}_{n-1}\\&\boldsymbol{C}^{\mathrm{T}}\dot{\boldsymbol{U}}_n=1\end{aligned} \tag{29}$$

where

$$\begin{aligned}&\tilde{\boldsymbol{K}}=\boldsymbol{K}+\frac{1-\alpha}{\gamma\Delta t}\boldsymbol{M}\\&\boldsymbol{R}_{n-1}=\frac{1-\alpha}{\gamma\Delta t}\boldsymbol{M}\dot{\boldsymbol{U}}_{n-1}+\frac{1-\gamma-\alpha}{\gamma}\boldsymbol{M}\ddot{\boldsymbol{U}}_{n-1}\end{aligned} \tag{30}$$

A solution of the above equations may be symbolically expressed as

$$\dot{\boldsymbol{U}}_n = \lambda_n \tilde{\boldsymbol{K}}^{-1}\boldsymbol{C} + \tilde{\boldsymbol{K}}^{-1}\boldsymbol{R}_{n-1}$$
$$\lambda_n = \frac{1 - \boldsymbol{C}^{\mathrm{T}}\tilde{\boldsymbol{K}}^{-1}\boldsymbol{R}_{n-1}}{\boldsymbol{C}^{\mathrm{T}}\tilde{\boldsymbol{K}}^{-1}\boldsymbol{C}} \tag{31}$$

in each iterative step. The solution of Eq. (31) in each iteration is used in a feed-back loop to update the modified stiffness matrix $\tilde{\boldsymbol{K}}$. The converged solution of $\dot{\boldsymbol{U}}_n$ and λ_n under a suitable stopping criterion terminates an iteration loop in each time step. Acceleration and increment of displacement at each time step are calculated with the following equations:

$$\ddot{\boldsymbol{U}}_n = \frac{1}{\gamma\Delta t}(\dot{\boldsymbol{U}}_n - \dot{\boldsymbol{U}}_{n-1}) - \frac{1-\gamma}{\gamma}\ddot{\boldsymbol{U}}_{n-1}$$
$$\Delta\boldsymbol{U}_n = \boldsymbol{U}_n - \boldsymbol{U}_{n-1} = \Delta t\dot{\boldsymbol{U}}_{n-1} + \frac{1}{2}\Delta t^2[(1-2\beta)\ddot{\boldsymbol{U}}_{n-1} + 2\beta\ddot{\boldsymbol{U}}_n] \tag{32}$$

The solution set (31) and (32) are used to calculate $\tilde{q}(\dot{\boldsymbol{U}})$ as well as the deformed shape, the strain and the flow stress.

3. Numerical analysis

The dynamic formulation for limit analysis derived in the previous section has been implemented into a finite element analysis code. The validity of the code has been examined in various numerical examples. The typical problem may be the high speed impact of a Taylor bar for bulk deformation and the dynamic crush of an S-rail for thin-wall deformation. Numerical results obtained from the present analysis are compared with those obtained from LS-DYNA3D. In order to evaluate the computational efficiency of the formulation developed, the computing time has been compared between the present analysis and the elasto-plastic explicit analysis with LS-DYNA3D.

3.1. Impact analysis of the Taylor bar

The Taylor impact test is a useful experiment to observe the material behavior at the high strain rates and evaluate dynamic material constitutive models. In this paper, the Taylor impact analysis with oxygen free, high conductivity (OFHC) copper is carried out with the dynamic limit analysis code developed. The dynamic material model of OFHC copper is expressed with the Johnson–Cook constitutive relation as shown in Eq. (10).

The material constants for OFHC copper are given in Table 1. When the material model of OFHC copper is considered as the quasi-static one, only the strain hardening term in Eq. (10) is applied to the analysis. The impact analysis result adopting the quasi-static model is compared with the one adopting the dynamic Johnson–Cook model.

The Taylor bar in the analysis has the length of 25.4 mm and the diameter of 7.62 mm. By virtue of symmetry, one quarter of the bar is considered in the numerical analysis. The finite element model consists of 864 eight-node solid elements and 1159 nodal points as shown Fig. 1. The initial impact velocity of the bar is 190 m/s and the interface between the bar and the rigid wall is assumed to be smooth.

Figs. 2 and 3 show the final deformed shapes of the Taylor impact bar with the Johnson–Cook material model and quasi-static model, respectively, comparing the present results with the elasto-plastic analysis results from LS-DYNA3D. The amount of deformation that is calculated with the Johnson–Cook model is

Table 1
Material constants in the Johnson–Cook constitutive relation for OFHC copper

Material	A	B	n	C	m	ρ	c_p	T_{melt}
OFHC copper	90 MPa	232 MPa	0.31	0.025	1.09	8940 kg/m^3	385 J/kg °C	1083 °C

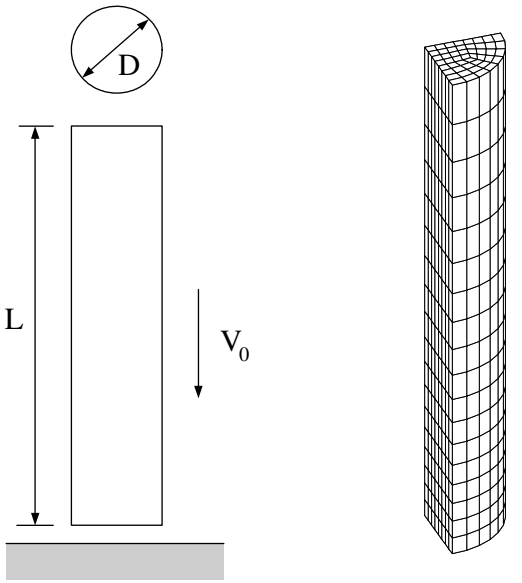

Fig. 1. Analysis conditions and finite element model for the Taylor impact bar.

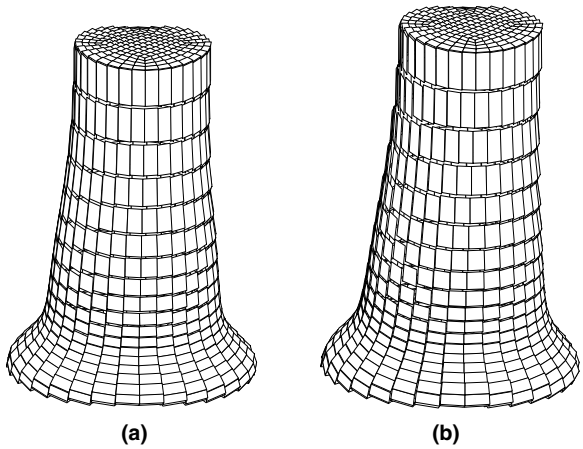

Fig. 2. Final deformed shapes of the Taylor impact bar with the Johnson–Cook material model: (a) limit analysis; (b) LS-DYNA3D.

smaller than that with the quasi-static model due to the strain-rate hardening effect. The deformed shape obtained from the dynamic limit analysis is similar to that from the elasto-plastic analysis with LS-DYNA3D.

The effective plastic strain distribution at the final deformed state is depicted in Figs. 4 and 5 in order to confirm the validity of the results by comparing them with the elasto-plastic analysis results obtained from LS-DYNA3D. The result from the present analysis shows fair coincidence to that from the elasto-plastic analysis. The maximum effective plastic strain at the impact end and the amount of deformation, however, tend to have a larger value in the result from the limit analysis than that from the elasto-plastic analysis as shown in Table 2. The difference of the deformation in Table 2 may be the result of that the dynamic limit analysis needs a finite value of the convergence criterion which terminates the iteration loop as well as it ignores the elastic deformation. The maximum effective plastic strain in the present analysis is about 2.18 at impact end for Johnson–Cook model in Table 2, which is a slightly larger value than the result of Johnson and Holmquist (1988). The deviation of the dynamic analysis result is 6.8% and the deviation of the quasi-static analysis result is 24.5%. This comparison demonstrates that dynamic limit analysis is necessary to predict the impact response correctly.

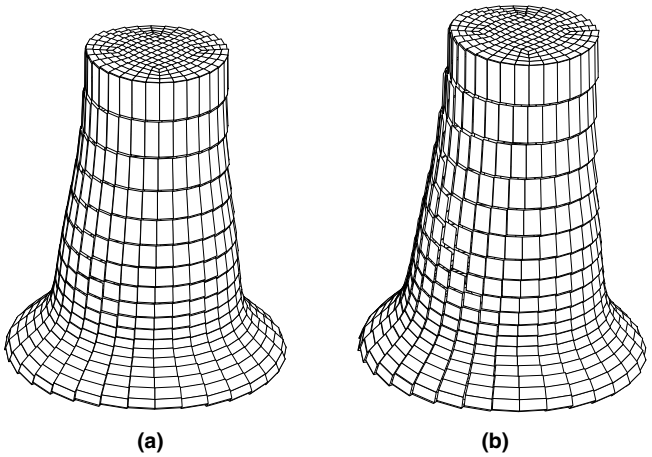

Fig. 3. Final deformed shapes of the Taylor impact bar with the quasi-static material model: (a) limit analysis; (b) LS-DYNA3D.

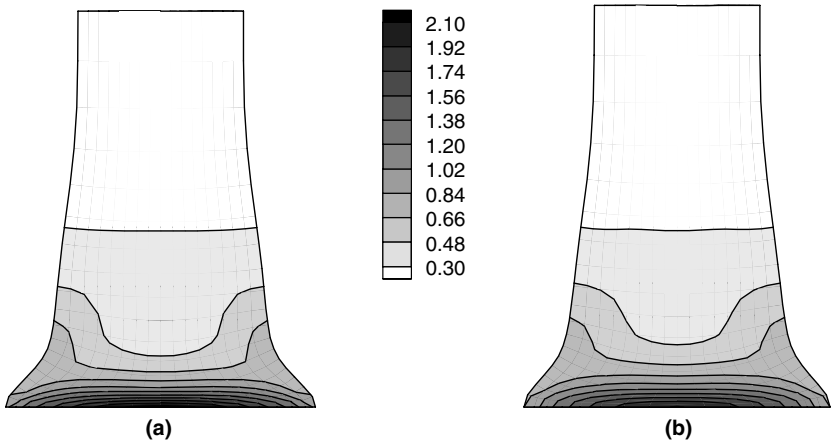

Fig. 4. Effective plastic strain distribution of the Taylor impact bar with the Johnson–Cook material model at final deformed state: (a) limit analysis; (b) LS-DYNA3D.

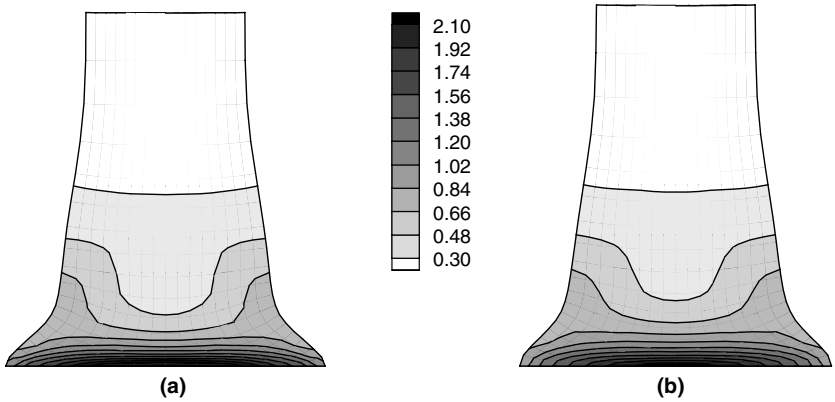

Fig. 5. Effective plastic strain distribution of the Taylor impact bar with the quasi-static material model at final deformed state: (a) limit analysis; (b) LS-DYNA3D.

Table 2
Comparison of deformation and the maximum effective plastic strain of the Taylor impact bar at the final deformed state: dynamic vs. quasi-static

Material model	Analysis tool	Final shape (mm)			Maximum effective plastic strain
		L	D	W	
Johnson–Cook model	Limit analysis	17.00	14.25	9.51	2.18
	LS-DYNA3D	17.29	14.08	9.53	1.93
Quasi-static model	Limit analysis	15.96	15.28	9.73	2.54
	LS-DYNA3D	16.22	14.92	9.75	2.21

W = Diameter of Taylor impact bar at $0.2L_0$ from the deformed end.
Maximum effective plastic strain in study of Johnson and Holmquist (1988) = 2.04.

The present analysis is not able to surpass the elasto-plastic explicit analysis in the computational efficiency in case that the size of the stiffness matrix is large and the stiffness matrix has a wide bandwidth such as this problem. It is because that the present analysis is an implicit analysis which needs to solve for the inverse of the stiffness matrix while the elasto-plastic explicit analysis does not need the inverse of the stiffness matrix. The computing time can be reduced dramatically by applying a more efficient linear solver than the skyline solver used in the present analysis.

3.2. Crush analysis of an S-rail

Crush analysis of an S-rail has been carried out with both the dynamic limit analysis and the elasto-plastic analysis in order to predict the load carrying capacity and the deformation modes. Fig. 6 shows the dimensions and the analysis condition for the crush analysis of an S-rail (Nikravesh and Chung, 1984; Drazetic et al., 1993). The finite element mesh system for the S-rail consists of 1024 four-node shell elements and 1105 nodal points. By virtue of symmetry, a half of the S-rail is considered in the analysis. One end is fixed

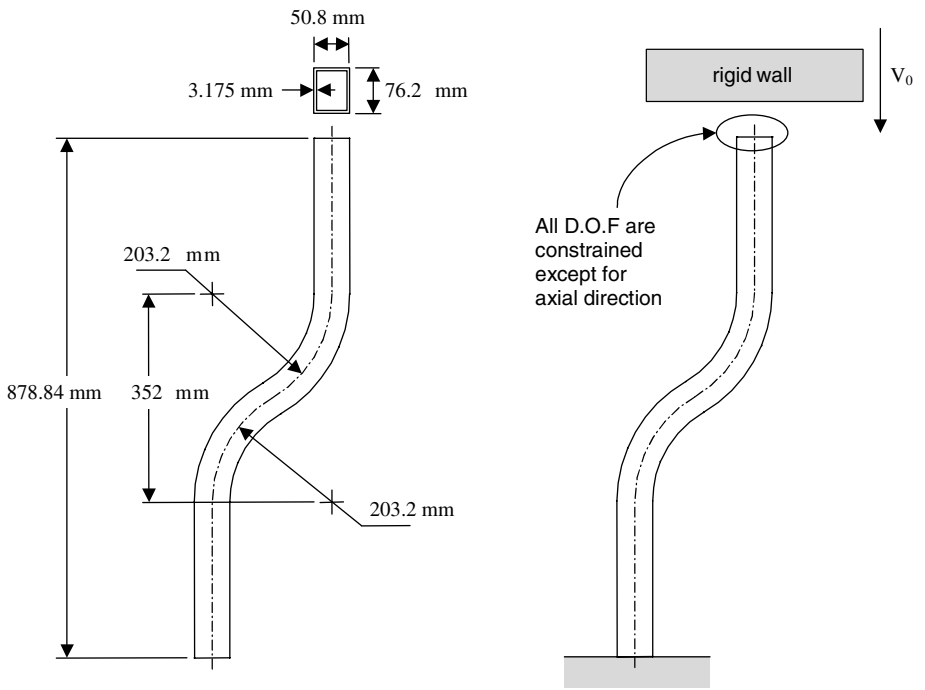

Fig. 6. Geometry, dimensions and boundary conditions of the S-rail.

and a moving rigid wall crash into the other end of the S-rail. The mass of the rigid wall is 200 kg and the initial impact velocity is 13.3 m/s. The material for the S-rail is SPCEN steel sheet, whose dynamic behavior can be expressed as the Johnson–Cook dynamic constitutive relation. The material constants for SPCEN steel sheet are given in Table 3. The flow stress of SPCEN is remarkably effected by the strain rate and the flow stress at the strain rate of 200/s is increased by 51% compared to that at the strain rate of 1/s. It is well demonstrated in Kang and Huh (2000) that the crash analysis of an auto-body has to be carried out considering the strain-rate hardening effect.

Deformed shapes obtained from the present analysis and the elasto-plastic analysis with LS-DYNA3D are shown in Figs. 7 and 8 at the crush time of 15 ms and 30 ms. Deformed shapes obtained from the two different analyses are very similar to each other except the deformation of the fixed region. The fixed end region

Table 3
Material constants in the Johnson–Cook constitutive relation for SPCEN steel sheet

Material	A	B	n	C	m	ρ	c_p	T_{melt}
SPCEN steel	201.1 MPa	459.8 MPa	0.528	0.097	0.3	7890 kg/m^3	472 J/kg °C	1487 °C

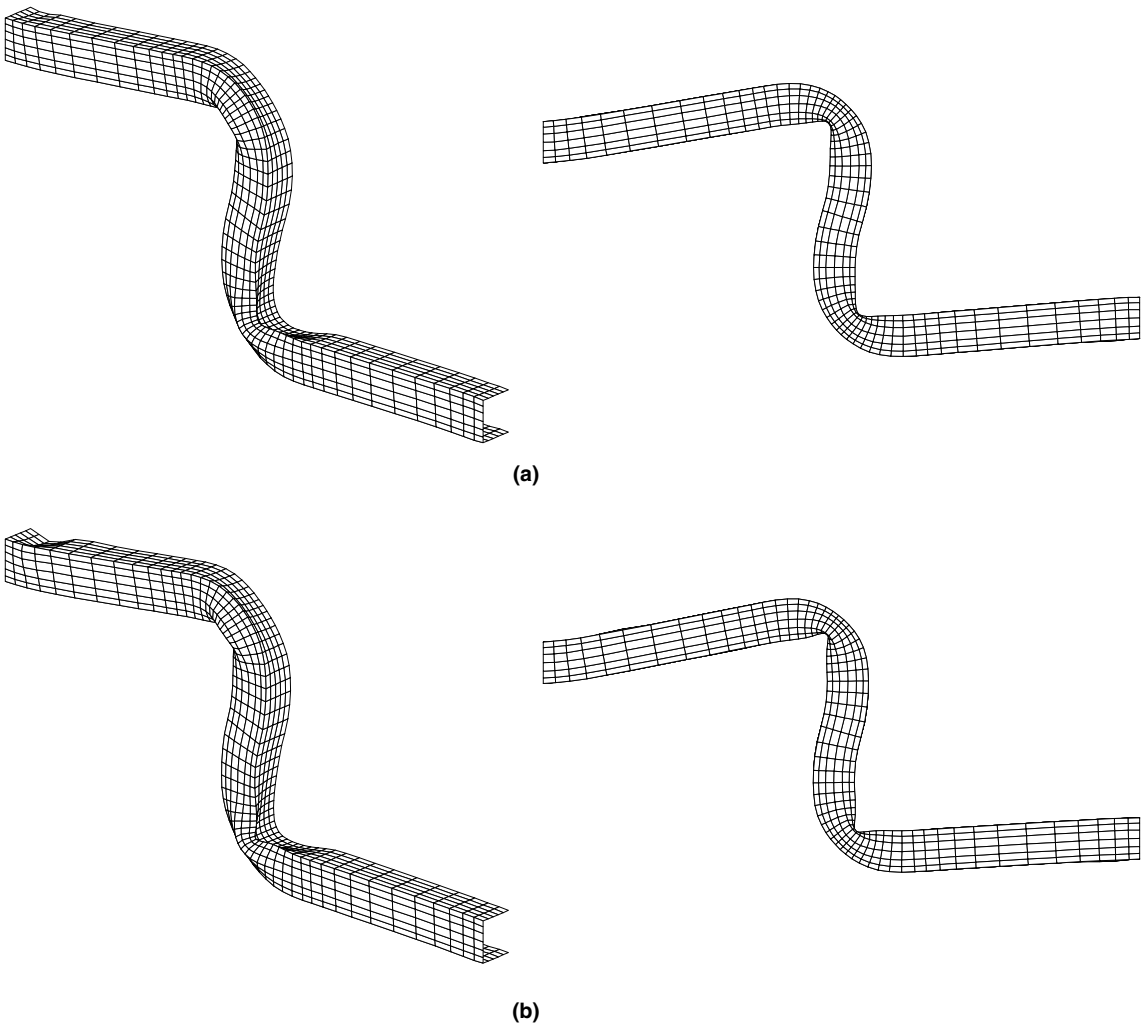

Fig. 7. Deformed shapes of the S-rail at 15 ms with the isometric view and the front view: (a) limit analysis; (b) LS-DYNA3D.

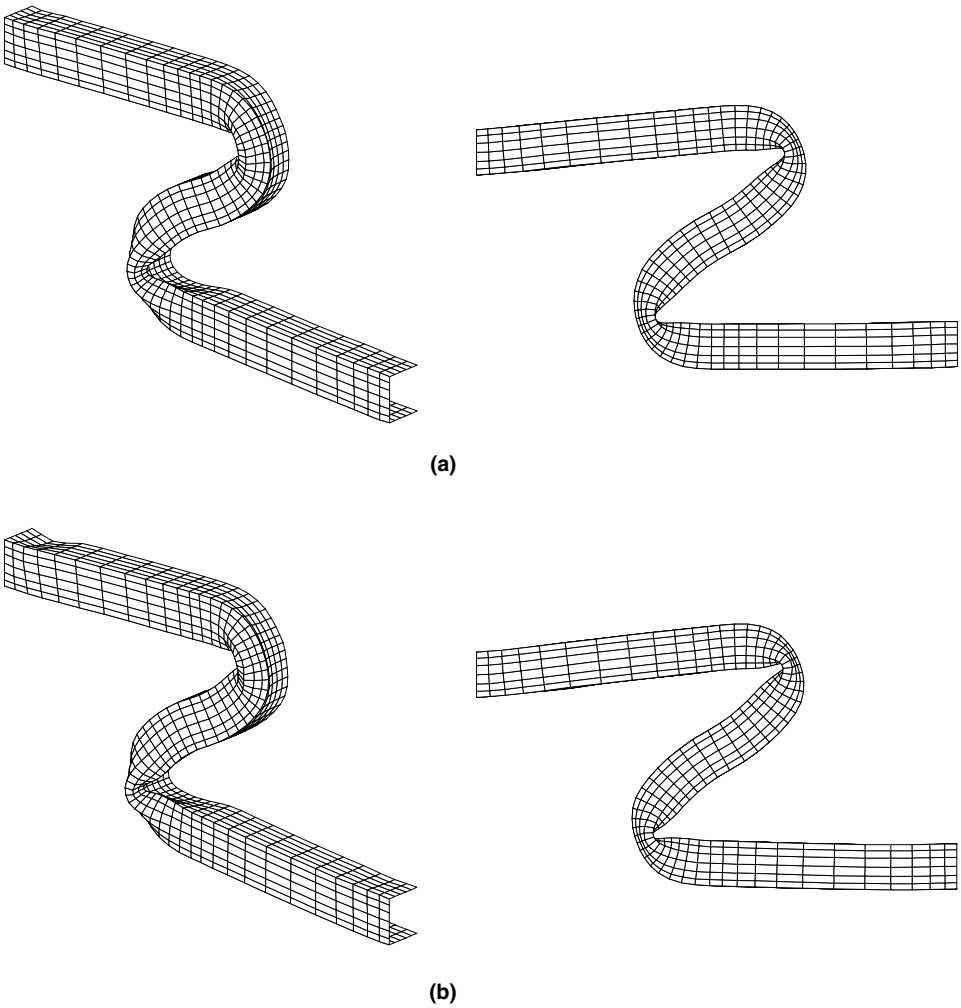

Fig. 8. Deformed shapes of the S-rail at 30 ms with the isometric view and the front view: (a) limit analysis; (b) LS-DYNA3D.

obtained from LS-DYNA3D undergoes more remarkable crush bending than one obtained from the present analysis. It is because the elastic wave prevails at the initial contact for crush. Compared to the elasto-plastic analysis, the limit analysis can only describe the plastic wave whose speed is lower than the elastic one. The plastic hinge is formed in two curved regions where deformation is concentrated. Since the plastic hinge is developed with the deformation, the collapse load starts to decrease after its initial peak at the beginning of crush. The two sequential dynamic collapse loads with respect to the displacement show fairly close tendency as shown in Fig. 9. The difference between two curves at the initial crush stage in Fig. 9 may result from the characteristic of limit analysis that ignores elastic deformation which is too much effective in the elasto-plastic analysis. Fig. 10 shows the absorbed energy during the deformation. The absorbed energy curve obtained from present analysis is almost same as one obtained from LS-DYNA3D.

To evaluate the computational efficiency, the computing time is compared between the present analysis and the elasto-plastic analysis with LS-DYNA3D as shown in Fig. 11 with the CPU time. These analyses were carried out on PC with INTEL PENTIUM4 1.9 GHz. Although elasto-plastic analysis tools were composed of very efficient routines, the present analysis was about 4.5 times faster than LS-DYNA3D as shown in Fig. 11. The comparison demonstrates that dynamic limit analysis results are reliable and can be efficiently used with remarkable savings of computing time to predict the sequential collapse load and collapse mode of structures under dynamic loading.

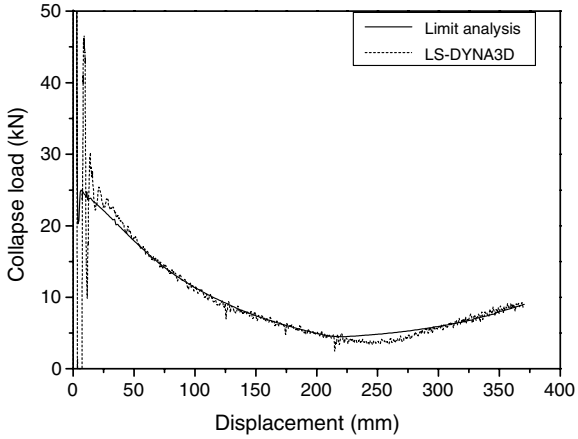

Fig. 9. Collapse load of the S-rail with respect to the displacement during the crush time of 30 ms.

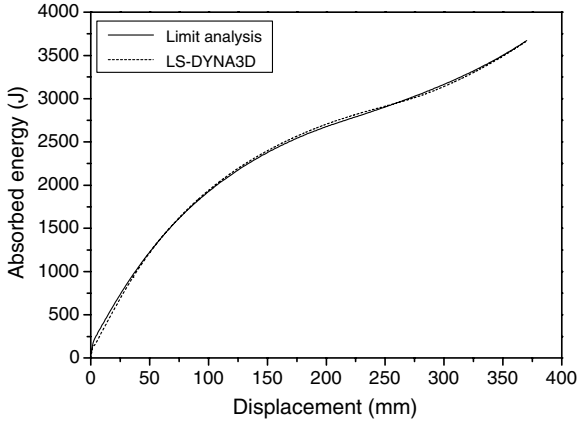

Fig. 10. Energy absorbed to the S-rail with respect to the displacement during the crush time of 30 ms.

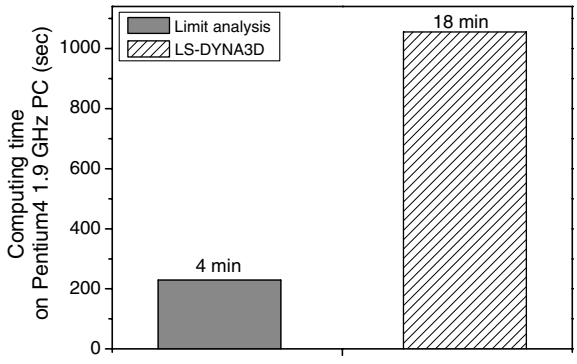

Fig. 11. Comparison of the computing time for the crush analysis of the S-rail.

4. Conclusion

This paper introduces a dynamic limit analysis formulation for calculating the dynamic response of structural members. A dynamic formulation for limit analysis has been derived for incremental analysis dealing

with the dynamic equilibrium condition, the time integration and dynamic material behavior. The time dependent term in the formulation is integrated with the WBZ-α time integration method. The dynamic material behavior is described as the Johnson–Cook model in order to consider the strain-rate hardening and the thermal softening as well as the strain hardening. The present method is a numerical tool predicting the dynamic collapse load, the collapse mechanism and the energy absorption efficiency for the crashworthiness of structures.

Impact analyses of the Taylor bar and an S-rail have been carried out to verify the validity and accuracy of the present dynamic limit analysis method. Analysis results were compared to elasto-plastic explicit analysis results obtained from LS-DYNA3D in order to evaluate its validity and accuracy. The comparison shows good coincidence in the deformation mode, the distribution of the effective plastic strain and the load-carrying capacity. Computational efficiency of the present analysis is greatly improved for thin-walled structures such as an S-rail in comparison with elasto-plastic explicit analysis. Results demonstrate that the dynamic limit analysis method is an effective and useful tool in the dynamic analysis and prediction of the crashworthiness of structural members.

References

Anderheggen, E., Knöpfel, H., 1972. Finite element limit analysis using linear programming. International Journal of Solids and Structures 8, 1413–1431.

Capsoni, A., Corradi, L., Vena, P., 2001. Limit analysis of anisotropic structures based on the kinematic theorem. International Journal of Plasticity 17, 1531–1549.

Christiansen, E., 1981. Computation of limit load. International Journal for Numerical Methods in Engineering 17, 1547–1570.

Christiansen, E., Andersen, K.D., 1999. Computation of collapse states with von Mises type yield condition. International Journal for Numerical Methods in Engineering 46, 1185–1202.

Christiansen, E., Pedersen, O.S., 2001. Automatic mesh refinement in limit analysis. International Journal for Numerical Methods in Engineering 50, 1331–1346.

Dang Hung, N., 1976. Direct limit analysis via rigid–plastic finite elements. Computer Methods in Applied Mechanics and Engineering 8, 81–106.

Drazetic, P., Markiewicz, E., Ravalard, Y., 1993. Application of kinematic models to compression and bending in simplified crash calculations. International Journal of Mechanical Sciences 3/4, 179–191.

Huh, H., Yang, W.H., 1991. A general algorithm for limit solutions of plane stress problems. International Journal of Solids and Structures 28 (6), 727–738.

Huh, H., Lee, C.H., Yang, W.H., 1999. A general algorithm for plastic flow simulation by finite element limit analysis. International Journal of Solids and Structures 36, 1193–1207.

Huh, H., Kim, K.-P., Kim, H.S., 2001. Collapse simulation of tubular structures using a finite element limit analysis approach and shell elements. International Journal of Mechanical Sciences 43, 2171–2187.

Johnson, G.R., Cook, W.H., 1983. A constitutive model and data for metals subjected to large strains, high strain rates and high temperatures. In: Proceedings of the Seventh International Symposium on Ballistics, The Hague, The Netherlands, pp. 541–547.

Johnson, G.R., Holmquist, T.J., 1988. Evaluation of cylinder-impact test data for constitutive model constants. Journal of Applied Physics 64 (8), 3901–3910.

Kang, W.J., Huh, H., 2000. Crash analysis of auto-body structures considering the strain-rate hardening effect. International Journal of Automotive Technology 1 (1), 35–41.

Kim, H.S., Huh, H., 1999. Vehicle structural collapse analysis using a finite element limit method. International Journal of Vehicle Design 21 (4), 436–449.

Nikravesh, P.E., Chung, I.S., 1984. Structural collapse and vehicular crash simulation using a plastic hinge technique. Journal of Structural Mechanics 12 (3), 371–400.

Ponter, A.R.S., Fuschi, P., Engelhardt, M., 2000. Limit analysis for a general class of yield conditions. European Journal of Mechanics A/Solids 19, 401–421.

Wood, W.L., Bossak, M., Zienkiewicz, O.C., 1981. An alpha modification of Newmark's method. International Journal for Numerical Methods in Engineering 15, 1562–1566.